JOURNAL OF MATERIALS SCIENCE 18 (1983) 1773–1784

Local melting of nodular cast iron by plasma arc

T. ISHIDA
The Research Institute for Iron, Steel and Other Metals, Tohoku University, Sendai, Japan

The microstructural changes in the fusion boundary area of nodular cast iron (NCI) were investigated by plasma arc local-melting with and without a filler metal. The NCI cylinder specimen was locally melted by the static plasma torch for a very short time, adopting the non-keyhole method. The microstructures produced in the fusion region, fusion boundary region and heat-affected zone (HAZ) were examined metallographically. In the absence of filler metal, the fusion boundary area is composed of ledeburite in the fusion region, and martensitic, troostitic–ferritic layers for the short arc-time and sorbitic, sorbitic–ferritic layers for long arc times in HAZ. Although the formation of white iron in the fusion region may be caused by a relatively high cooling rate, the major cause is due to supercooling effects produced by the decrease of magnesium content in the molten iron directly under the plasma arc. Using nickel and Ni–Fe filler metals, Ni-martensite appears in the deposited fusion boundary, and the HAZ region is composed of ledeburitic and martensitic or sorbitic layers. The ledeburitic layer thickness varies with the melting point of the filler metal. The diffusion of nickel from the deposit metal to the HAZ occurs at least until the fused base metal in the HAZ.

1. Introduction

It has recently been shown that the metal surface melting method using high-power energy produces a highly refined and homogeneous microstructure [1, 2] and gives adequate and rapid heat-treatment [3–5]. In this investigation, a basic study on the plasma arc welding of cast iron was undertaken; the fusion boundary microstructure of the localized melting of nodular cast iron (NCI) by plasma arc with high energy was examined.

The arc welding microstructure of NCI is characterized by the formation of white cast iron and martensitic layers in the heat-affected zone (HAZ) [6, 7]. Iron carbide forms in the fused base metal adjacent to the fusion zone due to a fast cooling rate and the absence of effective nuclei for the graphite during the solidification. High carbon martensite forms near the fused base metal due to the rapid cooling rate and the result of dissolution of carbon from the graphite nodule into the austenitic matrix. Although the formation of the carbide and the martensite, conventionally, is to be avoided by the use of moderate preheating and as slow a cooling rate as possible [7], the high energy plasma arc may possibly hinder this formation. The characteristic features of the ionization phenomenon under the plasma arc [8, 9] may be expected to be useful for the improvement of the structure of the cast iron weld interface.

The present research has been carried out to determine the microstructural changes in the fusion zone, the fusion boundary and the heat-affected zone (HAZ) of NCI produced by plasma arc local-melting with and without filler metal, adopting the non-keyhole method where the molten pool is dug down by the plasma arc and the arc disappears before the pool arrives at the under face, and specifically to obtain basic knowledge about the plasma arc of spheroidal graphite cast iron.

2. Experimental method

The chemical composition of the NCI investigated was 3.18 wt % C, 3.04 wt % Si, 0.30 wt % Mn, 0.023 wt % P, 0.010 wt % S and 0.032 wt % Mg.

0022–2461/83 $03.00 + .12

NCI was produced by reduction melting in an electric furnace, adding steel scrap to pig iron. The iron was magnesium-treated, and cast into a sand mould 40 mm in diameter. The predominant microstructure in these castings is a pearlitic–ferritic matrix with spheroidal graphite. Castings were cut into specimen cylinders 35 mm in diameter and 25 mm in length. In the use of filler metal, pure nickel and 50% Ni–50% Fe were employed as filler metals. These metals were provided from 10 mm diameter metal mould castings with deoxidized and degassed vacuum-melting of electrolytic nickel and iron. The filler metal used in this experiment was forged and rolled wire rod with a 4 mm diameter and 200 mm long.

The heat source for the local arc-melting was a transferred plasma arc welder (Hitachi, 300A). The base metal cylinder placing at the copper plate (15 mm x 100 mm x 100 mm) situated on the iron table was melted locally under the static plasma torch at fixed time intervals. When the filler metal was used it was inserted into the plasma arc and deposited onto the base metal. Arc time measurement was done simultaneously with the transfer of the main arc. Plasma arc-time, i.e. the occurrence time of the main arc, was from 10 to 40 sec. The welding current was 130 A, the plasma gas was argon with a flow rate of 2.8 $dm^3\ min^{-1}$, and the shielding gas was Ar + 10% H_2, with a flow rate of 13.0 $dm^{-3}\ min^{-1}$. The electrode used was tungsten with a 6.0 mm diameter and a nozzle diameter of 3.0 mm. The distance from the nozzle to the base metal was 8 to 10 mm. The shielding gas came out at a fixed time after the disappearance of the arc.

After local arc-melting was carried out and the specimens were cooled to room temperature on the iron table, they were cross-sectioned, polished and finished until a mirror face was obtained, and finally etched with 5% nital. Those with filler metal deposit were analysed across the deposit fusion boundary region with the help of electron probe microanalysis (EPMA).

Measurement of the temperature was undertaken to obtain cooling curves by plunging a 0.5 mm diameter Pt/Pt–13% Rh thermocouple directly into the molten pool after the arc had just disappeared. Cooling curves were recorded on a continuous chart recorder and the average cooling rate for each specimen was obtained during the temperature drop from 1200 to 750° C. The value of the cooling rate obtained was from 100 to 113.3° C sec^{-1} for an arc time of 15 to 20 sec and was from 33.3 to 36.3° C sec^{-1} for an arc time of 30 to 35 sec.

3. Results

3.1. In the absence of filler metal

3.1.1. Short arc-time

Fig. 1a shows the solidified microstructure of the fusion boundary area after exposure for 10 sec to the plasma arc. The average cooling rate in the

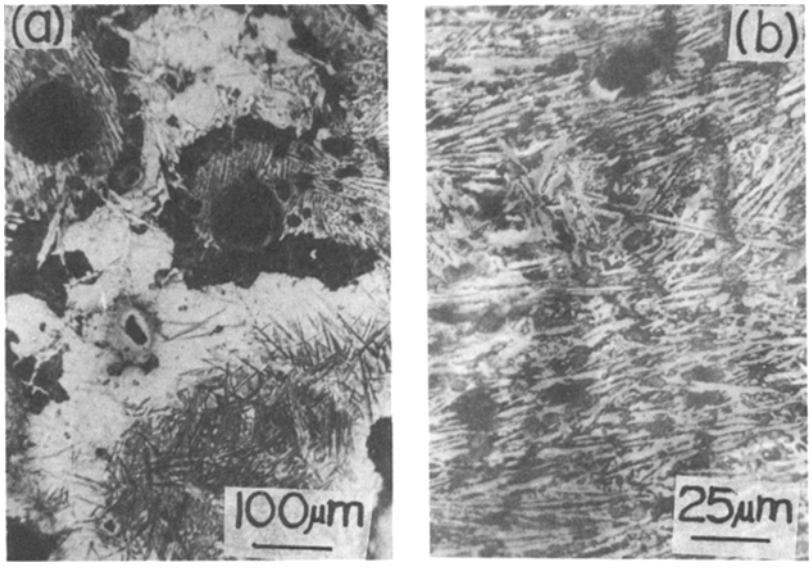

Figure 1 Microstructures of fusion boundary area and fusion region for 10 sec by plasma arc. (a) Fusion boundary area. (b) Fusion region.

fusion region is 107° C sec^{-1}. The fusion region has a ledeburitic structure and the HAZ has a martensitic one. Each portion obtained is described below.

3.1.1.1. Fusion region. Fig. 1b shows the complete fusion region as having a ledeburitic structure. Throughout the fusion region, a small amount of nodular graphite is recognized in the ledeburitic eutectic, but at the centre of the fusion region, in the vicinity of the fusion boundary region, evidence of graphite cannot be found.

3.1.1.2. Fusion boundary region. As shown in Fig. 2a, the portion bordering between the ledeburitic structure of the fusion region and the martensitic matrix of HAZ should be considered as a fusion line demarcated by troosite. In the case of the remaining undissolved graphite nodules on the fusion line, as shown in Fig. 2b, a small graphite nodule dissolving into the austenitic matrix is surrounded by a ledeburitic structure, then by troostite and then martensite of HAZ.

3.1.1.3. HAZ

3.1.1.3.1. White martensitic region or partial fusion region. The layer immediately adjacent to the fusion line has a matrix of white martensite which is easily unaffected by the etchant. In a graphite nodule existing further out the structure, in this case is: nodule, ledeburite, troostite, martensite (see Fig. 3a). This region represents the partial portion of the matrix of the base metal adjacent to the graphite melted during the heating cycle, while the remainder of the matrix is transformed to austenite. Both the partial melted liquid and the austenite were carbon-enriched. On cooling, the liquid transformed to massive iron carbide and the high carbon austenite transformed to coarse martensite.

3.1.1.3.2. Dark martensitic region. A short distance away from the fusion line, as shown in Fig. 3b, a graphite nodule directly adjoins the martensite where it becomes finer with increasing distance from the fusion line. In this region, no melting occurs and the carbon content in the austenitic matrix depends on the heating temperature and increases with the approach to the fusion line.

3.1.1.3.3. Troostite and ferrite-mixed region. Further away from the fusion line, as shown in Fig. 3c, the structure of the matrix is troostite (in this case needle martensite is not observed), and further away still a mixture of troostite with ferrite is observed. Then, as can be seen in Fig. 3d, there is thin ferrite and troostite around the graphite nodule, with coarser ferrite being precipitated further away in the matrix mixing of troostite and ferrite. In this region, dissolution and diffusion of carbon into the matrix particularly occur in the area around the graphite nodule and the matrix transforms to austenite. After cooling, troostite is precipitated in the surroundings of the

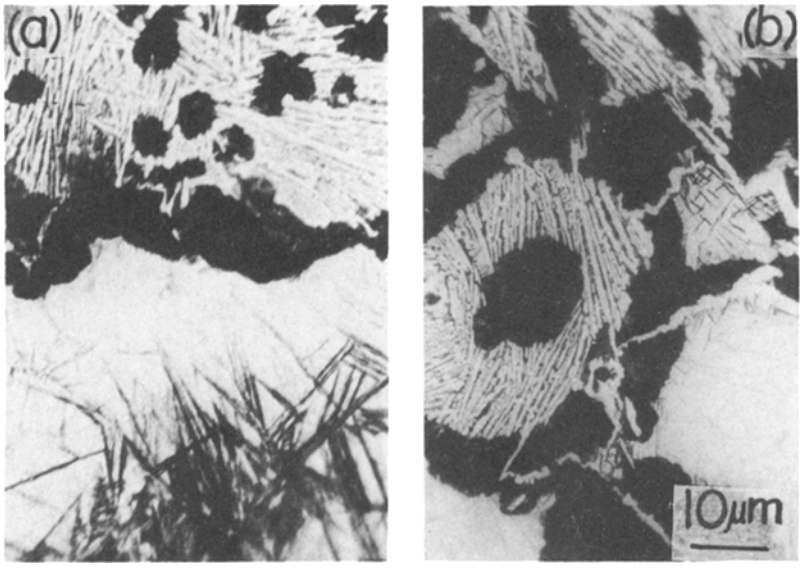

Figure 2 Microstructures of fusion line in fusion boundary region.

nodule and ferrite is observed at certain positions, carbon migration having scarcely occurred. On the base metal side, greater amounts of ferrite are found around the graphite nodule and thus troostite is scattered, as can be seen in Fig. 3e.

3.1.1.3.4. Ferrite and sorbitic pearlite structure. As shown in Fig. 3f, ferrite exists around the graphite nodule, on the other hand, pearlite becomes sorbitic in form.

The results of layer thickness and Vickers microhardness of each portion in HAZ are presented in Table I.

3.1.2. Long arc-time

Fig. 4a shows a solidified microstructure of the fusion boundary area treated for 29 sec with the plasma arc. The structure of the fusion region is white cast iron and as that of HAZ sorbite. The temperature in the fusion region increases with the large heat input due to the longer arc-time and the cooling rate of this region is around 34.7° C sec^{-1}. The results are described in the following sections.

3.1.2.1. Fusion region. The complete fusion region directly under the plasma arc has a ledeburitic

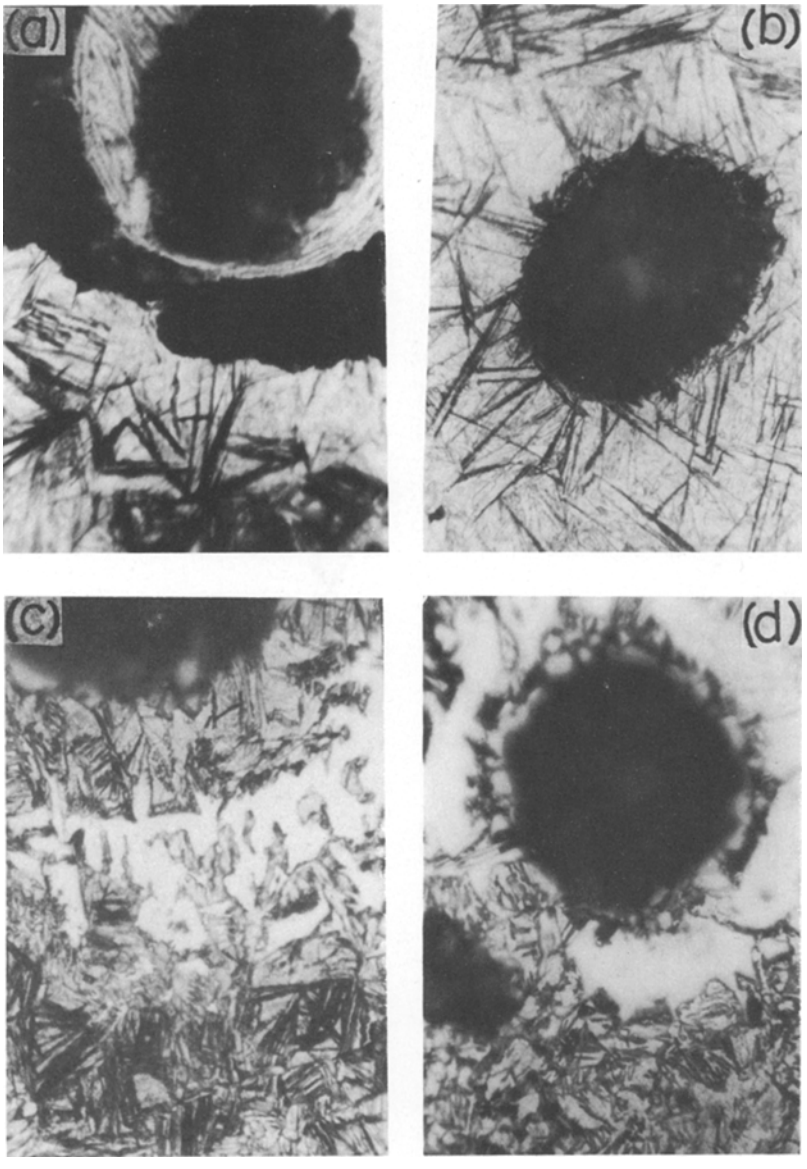

Figure 3 Microstructures of martensitic, troostitic–ferritic and ferritic–sorbitic pearlite layers in HAZ.

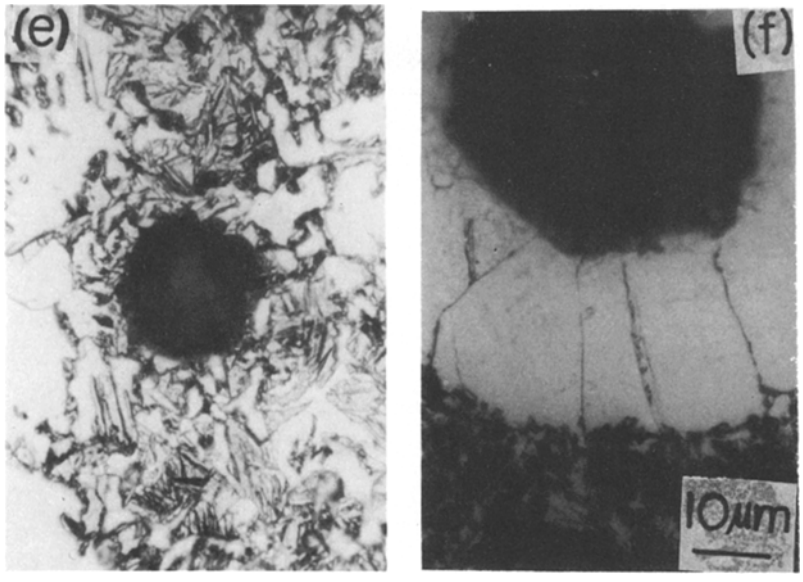

Figure 3 Continued.

structure in which some graphite crystallizes in the centre of the region (Fig. 4b). Graphite also forms at their edges of this region. The structure of this ledeburite is considered to be that of hypereutectic white cast iron.

3.1.2.2. Fusion boundary region. The portion bordering between the ledeburite and sorbite is the fusion line, as shown in Fig. 5a. Rapid dissolution of carbon from the graphite nodule into the surroundings occurs on the fusion line, as seen in Fig. 5b, resulting in a liquid due to the lowering of the melting point. This causes liquid cast iron to become ledeburite on solidification. Very tiny nodules of graphite are observed in the ledeburite. This is thought to be the newly crystallized graphite which forms during solidification when the original graphite dissolves and vanishes into molten iron.

3.1.2.3. HAZ

3.1.2.3.1. Partial fusion region. The structure of the matrix is sorbite. As can be seen in Fig. 6a, ledeburite around the graphite nodule is observed, but a white ferrite ring directly adjacent to the graphite nodule also appeared. In this region, the portion of the matrix near the graphite nodule melted during the heating cycle. It is recognized as a partial fusion region, and with a slow cooling rate the carbide surrounding each nodule deposited graphite onto the nodule leaving a ferrite ring. The matrix was a fine pearlite. Vickers hardness, H_v, in this region is 434.

3.1.2.3.2. Sorbite-scattered region. As can be seen in Fig. 6b, at a distance from the fusion line, ferrite is observed around the graphite nodule and the outer sorbite layer becomes scattered.

3.1.3. The structure and magnesium behaviour in the fusion region

The shape of the fusion region is a wine glass configuration characteristic of the plasma arc. Fusion volume and temperature increase with plasma arc-time. The matrix structure in the fusion region is ledeburite (Fig. 1b, Fig. 4b) in which the state of the graphite formation varies. For short arc-times in the centre of the upper fusion region the for-

TABLE I Average layer thickness and Vickers microhardness of each portion in HAZ

HAZ	Layer thickness (mm)		Hardness, H_v
	Centre	Near to edge	
White martensitic region	0.042	0.121	757
Dark martensitic region	0.389	1.247	642
Troostitic–ferritic structure	0.330	0.443	438

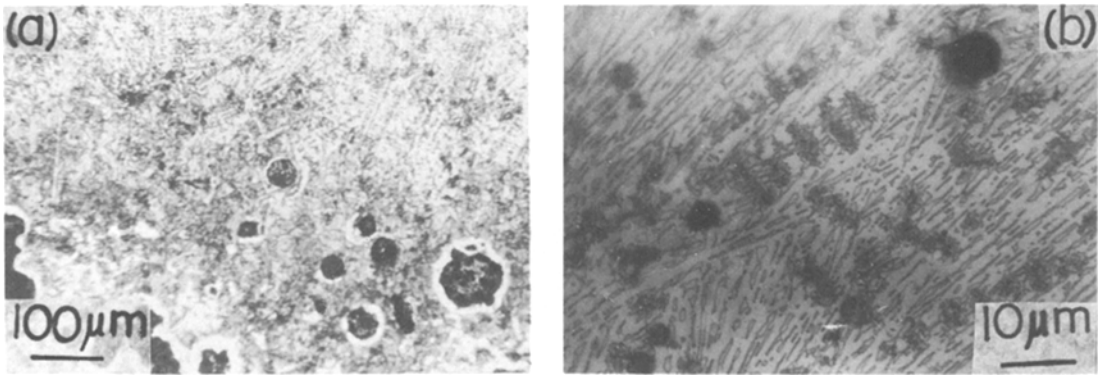

Figure 4 Microstructures of fusion boundary area and fusion region for 29 sec by plasma arc. (a) Fusion boundary area. (b) Fusion region.

mation of tiny graphite nodules was observed in the ledeburitic structure and for longer arc-times, in the upper fusion region greater amounts of graphite nodules which are smaller than the original graphite nodule, are formed in the structure. For any time in the neighbourhood of the fusion boundary of the lower fusion region, the formation of graphite nodules was not observed. As the cooling rate is very high in the neighbourhood of the fusion boundary adjacent to the unmelted base metal, iron carbide forms due to the absence of effective nuclei for graphite formation during solidification, and thus, the structure becomes hypereutectic white cast iron. In the case of the plasma arc, as the temperature of the molten metal increases suddenly and the primary graphite completely dissolves and vanishes into the melt, the graphite particle can be newly formed during solidification.

Fig. 7 shows the variation of magnesium in the fusion region with time. The reduced rate of magnesium is high in the initial period and the rate gradually lowers with time. A decrease of magnesium in molten cast iron causes a chilling effect which produces white iron. In spite of the slow cooling rate for longer arc-times, nodular graphite formation was observed, but this matrix structure becomes ledeburite due to the chilling effect.

3.2. Using filler metal

3.2.1. Nickel-filler metal

Fig. 8a shows the solidified microstructure of the deposited metal boundary area using pure Ni-filler metal.

3.2.1.1. Deposited metal. In the centre of the nickel deposited metal nodular and network graphites are formed in the nickel austenitic matrix. As can be seen in Fig. 8b, greater amounts of nodular graphite are formed in the neighbourhood of the deposited region. This suggests that great dissolution of base metal into the deposited metal occurs.

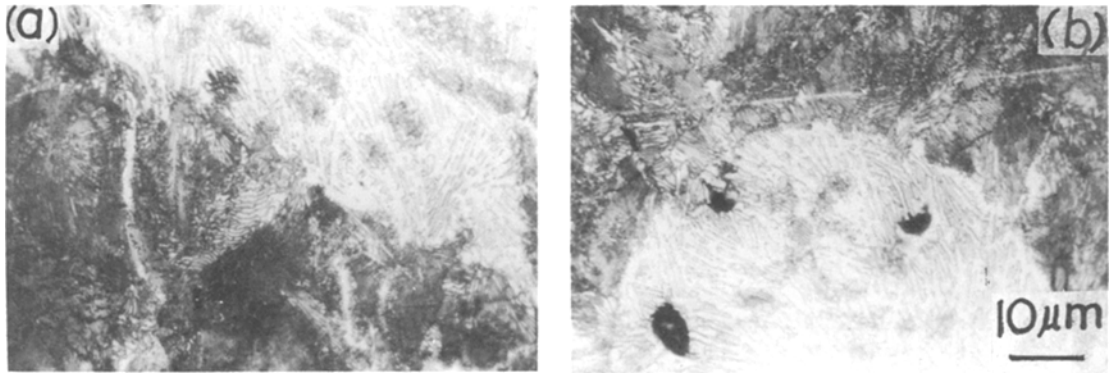

Figure 5 Microstructures of fusion line in fusion boundary region.

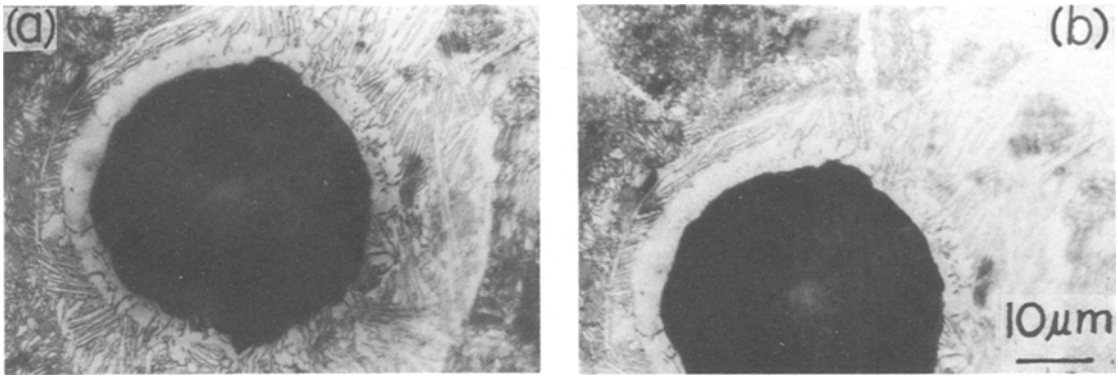

Figure 6 Microstructures of partial fusion region and sorbite-scattered region in HAZ.

3.2.1.2. Deposited boundary regions. As shown in Fig. 9a, the portion between the Ni-martensite and the ledeburite is the fusion line. Great amounts of nodular graphite are formed in Ni-martensite in which larger nodular graphites exist (Fig. 9b). These graphites may be precipitated directly from the liquid phase.

3.2.1.3. HAZ

3.2.1.3.1. Ledeburitic layer. As shown in Fig. 10a, the ledeburitic structure appears, on the whole, along the fusion line, in which great amounts of nodular graphite is formed. These graphite nodules are thought to be undissolved and newly-formed smaller graphite nodules. The mixing of ledeburite with fine pearlite around graphite nodules is detected in the ledeburitic structure, adjoining the sorbitic layer of the base metal side. As shown in Fig. 10b, ferrite and troostite rings can be recognized around the undissolving graphite nodule in the ledeburitic structure. The thickness of this ledeburitic layer is variable. The average value measure is indicated in Table II. The layer is thicker at the centre of the bead than at the circumference.

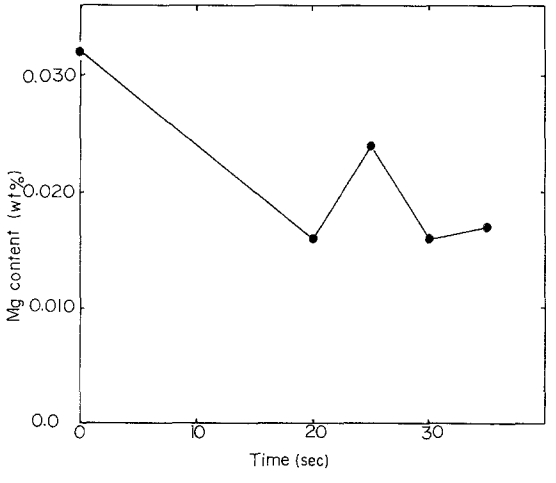

Figure 7 Loss of magnesium from fusion region of NCI by plasma arc local-melting.

3.2.1.3.2. Sorbitic layer. The matrix around the graphite nodule becomes a sorbitic structure.

3.2.1.3.3. Sorbite-scattered layer. The surroundings of the graphite nodule are ferritic and the structure of the matrix is sorbite–ferrite, that is, the sorbite becomes scattered.

3.2.1.3.4. Sorbitic pearlite layer. The structure of the matrix becomes sorbitic pearlite and ferrite.

3.2.2. Ni–Fe filler metal

Fig. 11a shows the solidified structure of the deposited fusion boundary area using 50% Ni–50% Fe filler metal.

3.2.2.1. Deposited metal. In Ni–Fe deposited metal, a small amount of graphite is formed in the Ni–Fe alloy matrix. As shown in Fig. 11b, the formation of Ni–Fe martensite and graphite nodules are observed in the neighbourhood of the fusion boundary of the depositing metal.

TABLE II Averaged thickness of ledeburitic layer in HAZ

Filler metal	Position in the section of bead in mm	
	Centre	Near to edge
Nickel	0.089	0.064
50% Ni–50% Fe	0.188	0.117

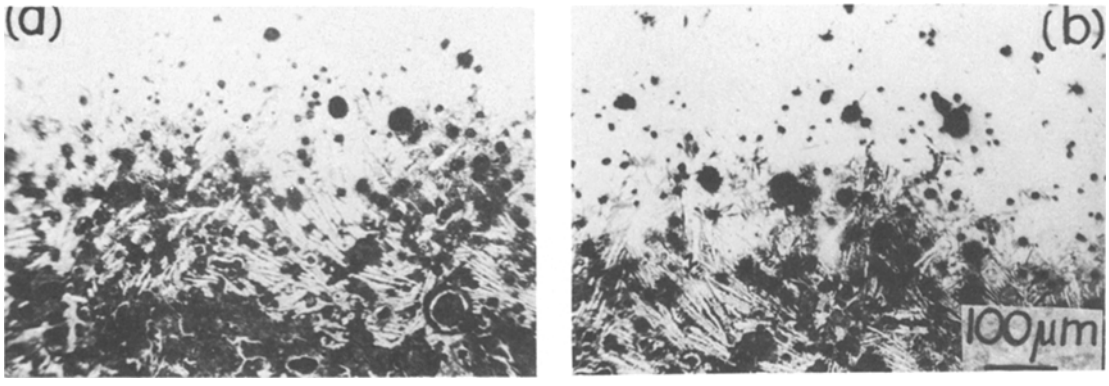

Figure 8 Microstructures of Ni-deposited fusion boundary area.

3.2.2.2. Deposited boundary region. The portion adjoining Ni–Fe martensite and ledeburite is the fusion line, as can be seen in Fig. 11c. Graphite nodules, in addition to Ni–Fe martensites, are crystallized.

3.2.2.3. HAZ

3.2.2.3.1. Ledeburitic layer. The ledeburitic structure along the fusion line, indicated in Fig. 11d, appears to be a thickening of the bead. A relatively small amount of nodular graphite is formed in the ledeburite eutectic. The ledeburitic layer is thicker at the centre of the bead than at the circumference, as indicated in Table II, and the layer thickness using Ni–Fe filler metal is about twice that of pure nickel.

3.2.2.3.2. Sorbitic layer. The portion adjoining the ledeburitic has a sorbite matrix, and ferrite around the graphite nodules is present further away from the fusion line.

3.2.2.3.3. Soribtic–ferritic layer. In this region sorbite is scattered with increasing ferrite the further the distance from the fusion line.

3.2.2.3.4. Pearlite–ferrite layer. The matrix becomes pearlite and ferrite. The pearlite becomes sorbitic.

3.2.3. Electron-probe microanalysis across deposited fusion boundary

Figs. 12 and 13 show the results of the EPMA traces across the deposited fusion boundary using nickel and Ni–Fe filler metals. A diffusion layer thickness of about 0.4 mm was observed across the fusion line. Nickel content in ledeburite of the HAZ changes and there is a concentration gradient in the ledeburite region. This fact indicates that nickel can diffuse from the deposited metal into the HAZ.

4. Discussion

Fig. 14 shows a schematic illustration of the solidified structure of the fusion boundary area by plasma arc local-melting with and without filler

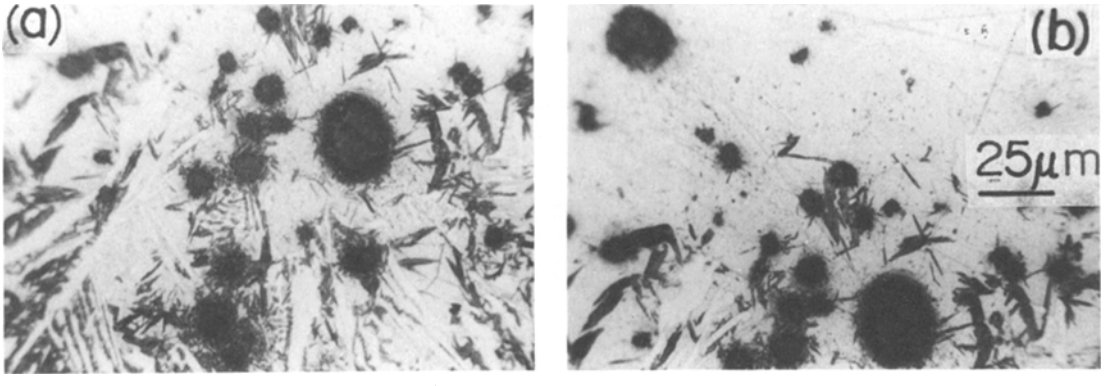

Figure 9 Microstructures of Ni-deposited boundary region.

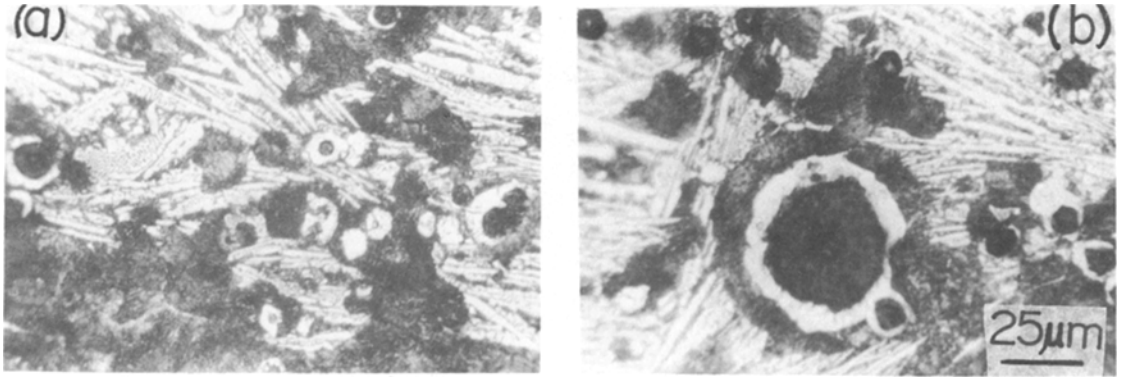

Figure 10 Microstructures of ledeburitic layer in HAZ.

metals. Further, terminology and morphology (microstructure) of discrete regions in a heterogeneous boundary are systematically described in Tables III and IV.

In the absence of a filler metal, as the plasma arc-time is very short, i.e. when the heat input is small, the cooling rate of the fusion boundary area is very high. For long-arc-times with larger heat inputs, a low cooling rate of the whole sample is obtained. In the case of local-melting without a filler metal, the structure of the fusion boundary area is that of ledeburite. It also appears in the fusion region. Martensitic and troostitic–ferritic layers are revealed in the HAZ when the arc-time is very short. Sorbitic and sorbitic–ferritic layers are revealed when arc-time is longer. In spite of a slow cooling rate with a long arc-time, the structure of the fusion region becomes white cast iron, i.e. a ledeburitic eutectic, though a relatively greater amount of graphite nodules exist in the

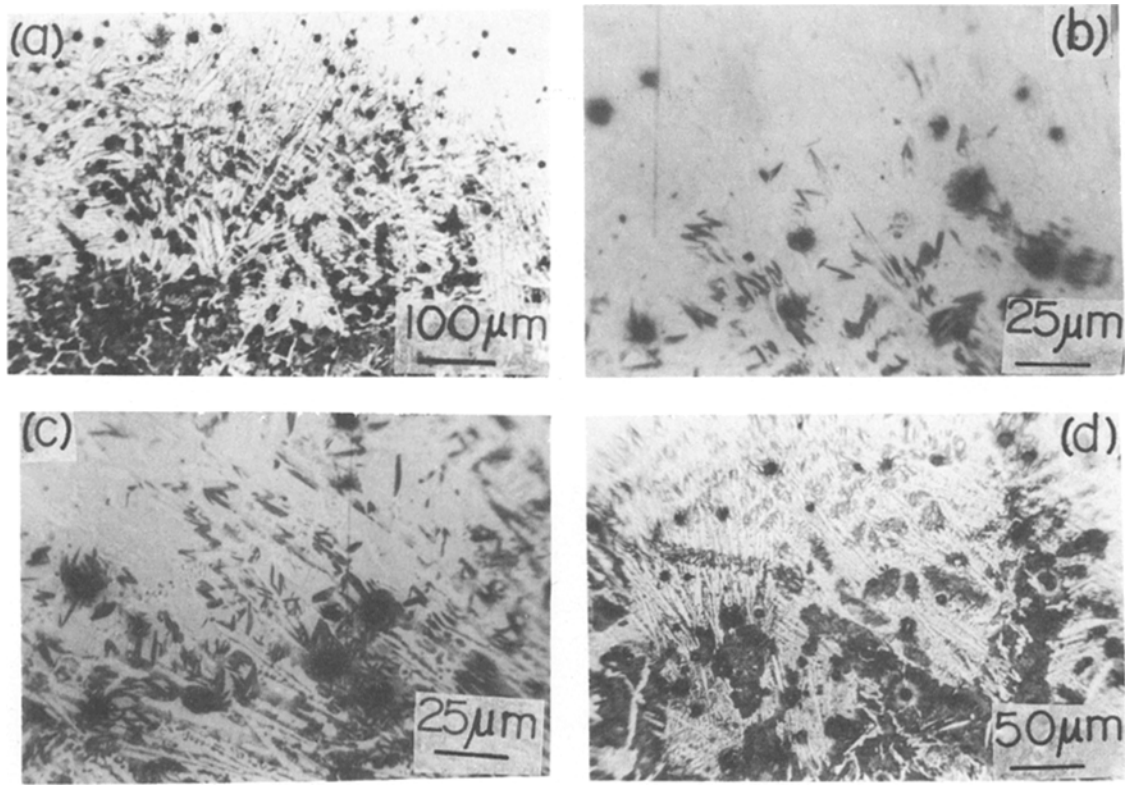

Figure 11 Microstructures of fusion boundary area with 50% Ni–50% Fe filler metal.

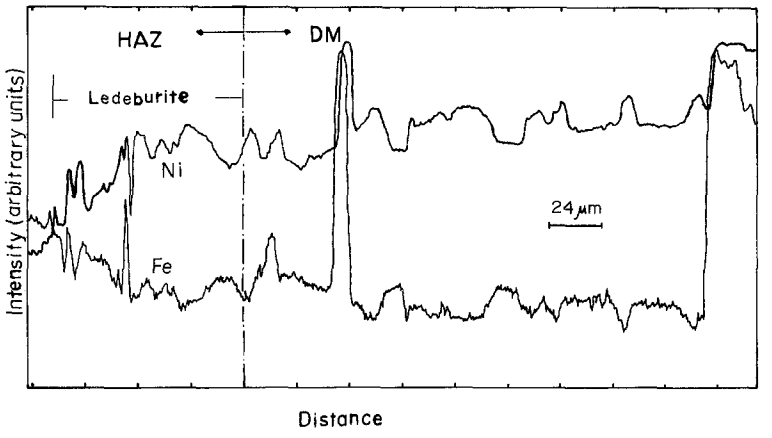

Figure 12 EPMA traces of Ni$K\alpha$ and Fe$K\alpha$ rays of NCI across fusion boundary region depositing pure nickel filler metal by plasma arc.

ledeburite. This phenomenon of becoming white iron produces a new supercooling effect as a result of the decrease of magnesium content in fusion region under the plasma arc. This phenomenon may be caused by the original behaviour of that residual magnesium in the molten iron [10, 11].

Using nickel and Ni–Fe filler metals, the deposited metal has a Ni–Fe–C alloy and Ni–martensite [12] appears in the deposited fusion boundary. HAZ is a region composed of a ledeburitic layer and martensitic or sorbitic layer. Ni–martensite formation is caused while the depositing metal dilutes the base metal. This results in a relatively uniform Ni–Fe–C content. At the deposited fusion boundary, Ni–martensite is apt to be formed by the process of supercooling due to the existence of either a stagnant layer or a laminar flow layer immediately adjacent to the base metal [13] and due to the accelerated region where more heat is transferred from the molten pool to the base metal. Great amounts of graphite are easy to precipitate in the deposited metal and the fusion boundary since nickel is unstable to Fe_3C and promotes graphitization.

The thickness of ledeburitic layer and replacement from the martensitic layer to the sorbitic layer are variable with the magnitude of the heat input from the deposited filler metal to the HAZ. This also suggests that the structure of HAZ changes with the differing melting points of the filler metals. The ledeburitic layer becomes thicker for Ni–Fe filler metal than for pure nickel, since the melting point of Ni–Fe alloy is slightly higher than that of pure nickel.

The diffusion of nickel in the deposited metal into the HAZ will be discussed later. It may be important to consider whether solute in the filler metal can actually diffuse into the HAZ or not. As can be seen in Figs. 12 and 13 by EPMA traces, nickel diffuses until the lebeburitic region is in the HAZ. On deposition the filler metal, the partial base metal, in the vicinity of deposited metal, begins to melt due to the heat from the deposited metal side. An interaction between the depositing metal and the partially fused base metal may play a role in the diffusion of nickel into the HAZ. Accordingly, the diffusion of nickel from the deposited metal into the HAZ occurs at least

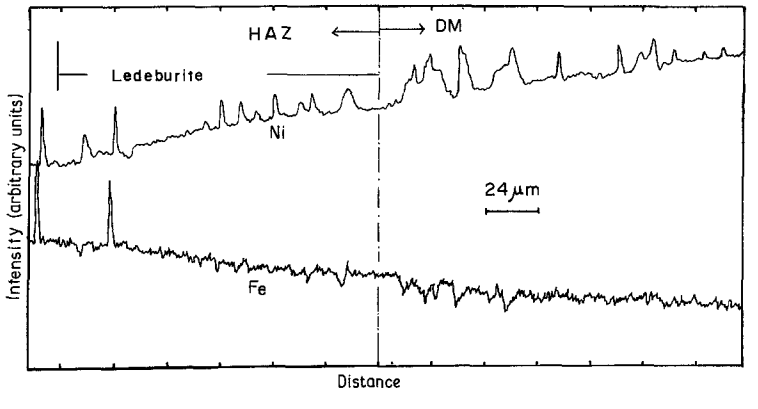

Figure 13 EPMA traces of Ni$K\alpha$ and Fe$K\alpha$ rays of NCI across fusion boundary region depositing Ni–Fe filler metal by plasma arc.

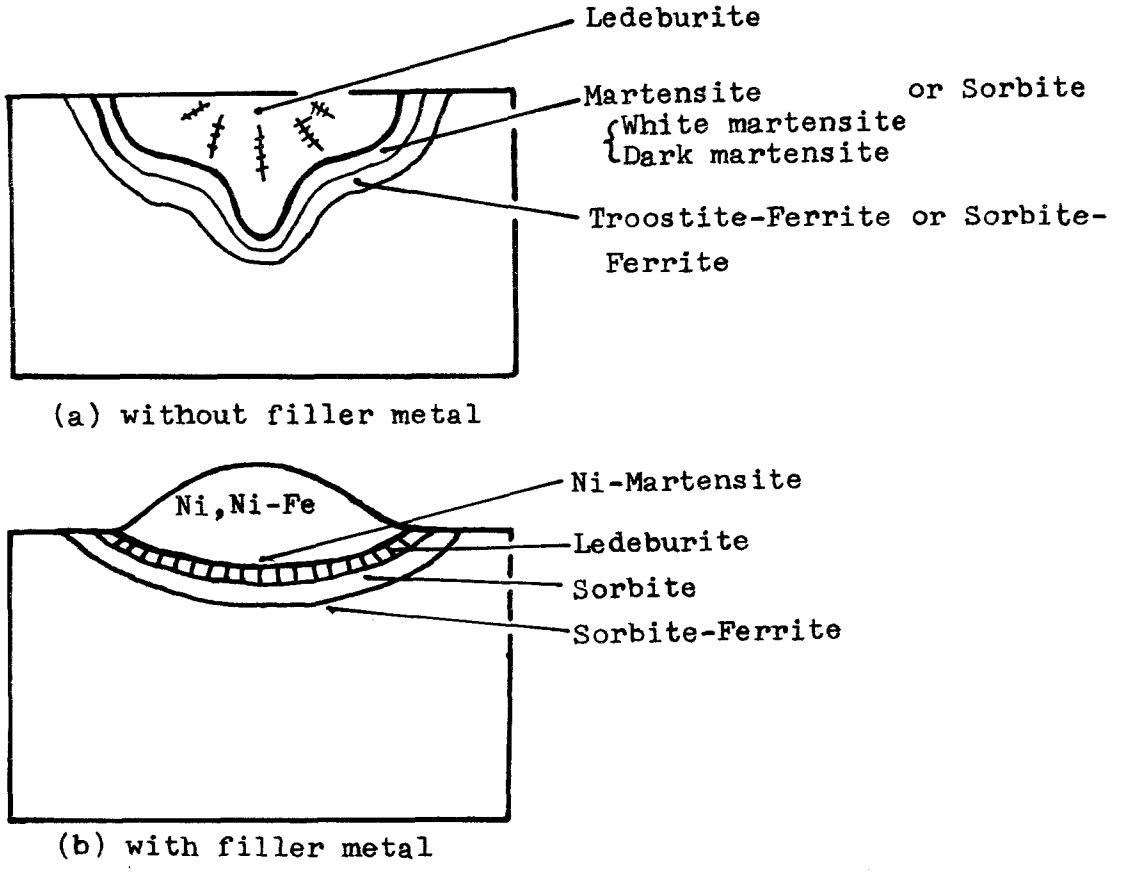

Figure 14 Schematic illustration showing solidified structure in fusion boundary area by plasma arc local-melting with and without filler metal.

until the fused base metal of HAZ. High nickel content in the ledeburitic region promotes graphitization of the liquid cast iron, therefore, the quantity of spheroidal nodules in the ledeburitic structures is more for the pure nickel filler metal than for Ni–Fe, as seen in Figs. 10a and 11d.

5. Conclusions

The microstructural changes in the fusion boundary area of the nodular cast iron have been investigated by plasma arc local-melting with and without a filler metal. The following main conclusions were reached:

TABLE III Terminology and morphology of discrete regions in heterogeneous boundary of NCI by plasma arc local-melting in the absence of filler metal

Terminology of portion of plasma arc melted zone	Morphology of discrete regions	
	Small heat input (High cooling-rate)	Large heat input (Low cooling-rate)
Fusion region (Completed melted region)	Ledeburite, tiny graphite nodule	Ledeburite, numerous tiny graphite nodules
Fusion boundary region (Fusion line)	Ledeburite, troostite	Ledeburite, sorbite
HAZ	Martensite, nodular graphite	Sorbite, nodular graphite
Partial fusion zone	White martensite, ledeburite	Sorbite, ledeburite
No fusion zone	Dark martensite, troostite–ferrite	Sorbite–ferrite

TABLE IV Terminology and morphology of discrete regions in heterogeneous boundary of NCI by plasma arc local-melting with filler metal

Terminology of portions of plasma arc melted zone	Morphology of discrete regions in the use of nickel and Ni–Fe alloy filler metals
Deposited metal	Ni–Fe–C alloy, tiny graphite nodule, network graphite
Fusion boundary region (Fusion line)	Ni-martensite, nodular graphite, ledeburite
HAZ	
Fusion zone	Ledeburite, tiny graphite nodule
Partial fusion zone	Ledeburite, troostite, nodular graphite
No fusion zone	Sorbite, sorbite–ferrite, nodular graphite

(a) In the absence of a filler metal, the structure of the fusion boundary area is composed of ledeburite in the fusion region and martensitic, troostitic–ferritic layers, for very short arc-times, and sorbitic, sorbitic–ferritic layers, for longer arc-times in the HAZ. In this martensitic layer, white and dark martensites were observed.

(b) In the fusion region, the production of white cast iron may occur due to the supercooling effect as a result of the decrease in the residual magnesium content under the plasma arc.

(c) Using nickel and Ni–Fe filler metals, Ni–martensite appears in the deposit fusion boundary and the HAZ region is composed of ledeburitic and martensitic or sorbitic layers. The ledeburitic layer thickness varies with the melting point of the filler metal.

(d) The diffusion of nickel from the deposit metal to the HAZ is able to occur at least as far as the fused base metal of the HAZ.

Acknowledgements

The author would like to thank Mr H. Yamaguchi (Hitachi Ltd.) for his help and advice in plasma arc experiment and Mr S. Oki for the EPMA work.

References

1. T. R. ANTHONY and H. E. CLINE, *J. Appl. Phys.* 49 (1978) 1248.
2. P. R. STRUTT, *Mater. Sci. Eng.* 44 (1980) 239.
3. W. HILLER, *Giesserei* 63 (1976) 316.
4. G. H. HARTH, W. C. LESLIE, V. G. GREGSON and B. A. SANDERS, *JOM* 28 (1976) 5.
5. G. J. OGILVIE and I. M. OGILVY, *Metals Forum* 2 (1979) 34.
6. E. E. HUCKE and H. UDIN, *Weld. J.* 32 (1953) 378s.
7. E. F. NIPPES, W. F. SAVAGE and W. A. OWCZARSKI, *ibid.* 39 (1960) 465s.
8. C. D. LUNDIN and W. J. RUPRECHT, *ibid.* 56 (1977) 1s.
9. C. B. SHAW, Jr, *ibid.* 59 (1980) 121s.
10. K. OKABAYASHI, *J. Jpn. Inst. Met.* 22 (1958) 73.
11. K. OKABAYASHI, *ibid.* 22 (1958) 77.
12. D. W. ZITZELSBERGER, *Schw. u. Schn.* 11 (1959) 416.
13. W. F. SAVAGE, E. F. NIPPES and E. S. SZEKERES, *Weld. J.* 55 (1976) 260s.

Received 20 September
and accepted 23 November 1982